LUND UNIVERSITY

Robust Phase-Based Positioning Using Massive MIMO with Limited Bandwidth

Li, Xuhong; Batstone, Kenneth John; Åström, Karl; Oskarsson, Magnus; Gustafson, Carl; Tufvesson, Fredrik

Published in:
28th Annual IEEE International Symposium on Personal, Indoor and Mobile Radio Communications, PIMRC 2017.

DOI:
10.1109/PIMRC.2017.8292362

2018

Document Version:
Peer reviewed version (aka post-print)

Link to publication

Citation for published version (APA):
Li, X., Batstone, K. J., Åström, K., Oskarsson, M., Gustafson, C., & Tufvesson, F. (2018). Robust Phase-Based Positioning Using Massive MIMO with Limited Bandwidth. In *28th Annual IEEE International Symposium on Personal, Indoor and Mobile Radio Communications, PIMRC 2017.* IEEE - Institute of Electrical and Electronics Engineers Inc.. https://doi.org/10.1109/PIMRC.2017.8292362

Total number of authors:
6

General rights
Unless other specific re-use rights are stated the following general rights apply:
Copyright and moral rights for the publications made accessible in the public portal are retained by the authors and/or other copyright owners and it is a condition of accessing publications that users recognise and abide by the legal requirements associated with these rights.
• Users may download and print one copy of any publication from the public portal for the purpose of private study or research.
• You may not further distribute the material or use it for any profit-making activity or commercial gain
• You may freely distribute the URL identifying the publication in the public portal

Read more about Creative commons licenses: https://creativecommons.org/licenses/

Take down policy
If you believe that this document breaches copyright please contact us providing details, and we will remove access to the work immediately and investigate your claim.

LUND UNIVERSITY

PO Box 117
221 00 Lund
+46 46-222 00 00

Download date: 08. Oct. 2022

Robust Phase-Based Positioning Using Massive MIMO with Limited Bandwidth

Xuhong Li[1], Kenneth Batstone[2], Kalle Åström[2], Magnus Oskarsson[2], Carl Gustafson[1], Fredrik Tufvesson[1]
[1]Dept. of Electrical and Information Technology, Lund University, Sweden.
[2]Centre for Mathematical Sciences, Lund University, Sweden.
Email: xuhong.li@eit.lth.se

***Abstract*—This paper presents a robust phase-based positioning framework using a massive MIMO system. The phase-based distance estimates of MPCs together with other parameters are tracked with an EKF, the state dimension of which varies with the birth-death processes of paths. The RIMAX and the modeling of dense multipath component in the framework further enhance the quality of parameter tracking by providing an accurate initial state and the underlying noise covariance. The tracked MPCs are fed into a time-of-arrival self-calibration positioning algorithm for simultaneous trajectory and environment estimation. Throughout the positioning process, no prior knowledge of the surrounding environment and base station position is needed. The performance is evaluated with the measurement of a 2D complex movement, which was performed in a sports hall with an antenna array with 128 ports as base station using a standard cellular bandwidth of 40 MHz. The positioning result shows that the mean deviation of the estimated user equipment trajectory from the ground truth is 13 cm. In summary, the proposed framework is a promising high-resolution radio-based positioning solution for current and next generation cellular systems.**

I. Introduction

High precision positioning information is a fundamental component of autonomous systems and location-aware applications in mobile devices. To pursue better user experience, these new services and systems keep bringing new challenges to the positioning systems regarding the accuracy, reliability, etc. The Global Positioning System (GPS) works well outdoors, but the accuracy and robustness degrade severely in scenarios like urban canyons and indoor environments due to poor propagation conditions between satellites and user equipment (UE). In contrast, cellular and wireless networks generally have good coverage in those GPS harsh environments. As a substitute or supplement to GPS, much effort has been put into the research of radio-based positioning techniques.

Accurate radio-based positioning commonly relies on geometrical information (distance, delay and angle) of multipath components (MPCs) from the radio channel. The estimation quality of these channel parameters in turn determines the positioning performance. In recent years, positioning with ultra-wideband (UWB) signal has drawn special interest because of the excellent accuracy [1]. The fine delay resolution due to the large bandwidth used makes it possible to resolve MPCs and track the distance changes in centimeter level. However, UWB positioning can only be applied in limited scenarios considering it is a low-power and short-range technique. These shortcomings naturally lead us to the question: is it possible to deliver comparable positioning accuracy by utilizing limited bandwidth in both indoor and outdoor scenarios? We try to solve the puzzle from a channel modelling perspective. The wireless propagation channel is commonly characterized as a sum of specular-like paths and non-resolvable components. Considering that cellular systems are typically operating with a carrier frequency at a few GHz with a bandwidth of 20-40 MHz, the delay resolution is in a scale of 7.5-15 m. However, we notice that the corresponding wavelengths are in the order of centimeters and one wavelength corresponds to a 2π phase shift. For each MPC, the delay and phase are two parameters which vary simultaneously with the wave propagating. If the spatial sampling rate of the radio channel is sufficiently high, i.e., taking a few snapshots within one wavelength movement, it is possible to track the distance change in centimeter level by measuring the phase shift between two consecutive snapshots. With limited bandwidth, the coherence in the delay domain is a challenge for successfully detecting and tracking many MPCs simultaneously. However, the large-scale antenna array could provide additional distinction between MPCs in the spatial domain. The feasibility of the phase-based positioning has been preliminarily proved in [2]. In that work, the phase and delay are assumed to be independent parameters, which are estimated separately and only the phase is used for the movement tracking. Because phase and delay affect each other with wave propagating, and phase estimates are usually discontinuous in complex environments, there are risks of causing errors or losing tracks.

Motivated by the above analysis, we present a robust phase-based positioning framework in this paper. As a proof-of-concept study, the focus of this work is on demonstrating the possibility of high-resolution radio-based positioning given limited bandwidth and with no prior environment knowledge, rather than on reducing system complexity to implement real-time positioning. Based on some well-established algorithms, e.g,. the Extended Kalman Filter (EKF) [3] and the iterative maximum-likelihood estimation algorithm (RIMAX) [4], the MPC parameters are extracted from the channel measurement data. A time-of-arrival (TOA) self-calibration positioning algorithm, which is a structure-of-motion approach and widely used in image processing, is finally applied for simultaneous UE trajectory and environment estimation. The main contributions are

978-1-5386-3531-5/17/$31.00 © 2017 IEEE

- The unique mapping between the phase shift and the distance change in our dynamic model leads to a simpler kinematic model by involving less parameters, and the robustness of the system is also improved.
- The performance is evaluated with real measurements of a complex movement. The results prove that the proposed framework provides outstanding MPC tracking and positioning performance even with limited bandwidth.

The paper is structured as follows. In Section II, dynamic propagation channel modeling is discussed. Section III introduces the estimation of path parameters with the EKF. Section IV describes details of the measurement campaign. The MPC tracking results are presented in Section V. Section VI introduces the TOA positioning algorithm and positioning result is presented. Finally, Section VII concludes the paper.

II. Dynamic Propagation Channel Modeling

An observation of the propagation channel, the impulse response $\mathbf{h}_k$ could be decomposed into three non-overlapping components: specular components $\mathbf{h}_{sp}$, dense multipath component (DMC) $\mathbf{h}_{dmc}$ and measurement noise $\mathbf{h}_n$, yielding

$$\mathbf{h}_k = \mathbf{h}_{sp} + \mathbf{h}_{dmc} + \mathbf{h}_n. \tag{1}$$

Positioning relies on the geometrical information from $\mathbf{h}_{sp}$, which is characterized as a superposition of MPCs. The other two components constitute measurement impairments for our purpose.

A. Channel Model

In the proposed framework, the double-directional radio channel model [5] is employed to extract the spatial and temporal information of the MPCs from the measured channel transfer function $\mathbf{H} \in \mathbb{C}^{N_s \times N_f \times N_{\mathrm{Tx}} \times N_{\mathrm{Rx}}}$, given as

$$\mathbf{H}(f) = \sum_{l=1}^{L} \boldsymbol{\gamma}_l e^{-j2\pi f \frac{d_l}{c}} \mathbf{G}_{\mathrm{Rx}}(\varphi_{\mathrm{Rx},l}, \theta_{\mathrm{Rx},l}) \mathbf{G}_{\mathrm{Tx}}(\varphi_{\mathrm{Tx},l}, \theta_{\mathrm{Tx},l})^{\mathrm{T}}, \tag{2}$$

where N_s, N_f, N_{Tx} and N_{Rx} refer to the number of channel snapshots, frequency sample points, transmit and receive antenna elements. $\mathbf{G}_{\mathrm{Tx}} \in \mathbb{C}^{N_{\mathrm{Tx}} \times N_a N_e}$ and $\mathbf{G}_{\mathrm{Rx}} \in \mathbb{C}^{N_{\mathrm{Rx}} \times N_a N_e}$ describe the far-field antenna response of all antenna array ports at the transmit and receive sides, with respect to the azimuth and elevation angles of departure (AODs) $(\varphi_{\mathrm{Tx},l}, \theta_{\mathrm{Tx},l})$ and angles of arrival (AOAs) $(\varphi_{\mathrm{Rx},l}, \theta_{\mathrm{Rx},l})$ of the lth path. N_a and N_e represent the number of azimuth and elevation angular samples. L is the number of propagation paths. The complex path weight is parametrized as $\boldsymbol{\gamma}_l = \boldsymbol{\alpha}_l e^{j\boldsymbol{\phi}_l}$ where $\boldsymbol{\alpha}_l$ and $\boldsymbol{\phi}_l$ represent the vectors of magnitude and phase, respectively. Instead of using delay, we directly interpret the phase shift as a distance measure, i.e., phase-based distance d_l. The time-variant structural vectors associated with the propagation environment geometry and the path weights are defined as

$$\boldsymbol{\mu} = [\boldsymbol{d}^{\mathrm{T}} \quad \boldsymbol{\varphi}_{\mathrm{Tx}}^{\mathrm{T}} \quad \boldsymbol{\theta}_{\mathrm{Tx}}^{\mathrm{T}} \quad \boldsymbol{\varphi}_{\mathrm{Rx}}^{\mathrm{T}} \quad \boldsymbol{\theta}_{\mathrm{Rx}}^{\mathrm{T}}], \tag{3}$$

$$\boldsymbol{\alpha} = [\boldsymbol{\alpha}_{\mathrm{HH}}^{\mathrm{T}} \quad \boldsymbol{\alpha}_{\mathrm{HV}}^{\mathrm{T}} \quad \boldsymbol{\alpha}_{\mathrm{VH}}^{\mathrm{T}} \quad \boldsymbol{\alpha}_{\mathrm{VV}}^{\mathrm{T}}], \tag{4}$$

$$\boldsymbol{\phi} = [\boldsymbol{\phi}_{\mathrm{HH}}^{\mathrm{T}} \quad \boldsymbol{\phi}_{\mathrm{HV}}^{\mathrm{T}} \quad \boldsymbol{\phi}_{\mathrm{VH}}^{\mathrm{T}} \quad \boldsymbol{\phi}_{\mathrm{VV}}^{\mathrm{T}}], \tag{5}$$

where $\{\mathrm{HH}, \mathrm{HV}, \mathrm{VH}, \mathrm{VV}\}$ represent four polarimetric transmissions, e.g., HV means horizontal-to-vertical transmission.

B. Dynamic Model

A discrete white noise acceleration model is used to describe the changes of propagation parameters [6], with the assumption that the motion and underlying noise process of different parameters are uncorrelated. The discrete-time state transition equation is expressed as

$$\mathbf{x}_k = \mathbf{F}\mathbf{x}_{k-1} + \boldsymbol{v}_k, \tag{6}$$

where $\boldsymbol{v}_k$ is state noise following zero mean normal distribution with the variance matrix $\mathbf{Q}$. The state transition matrix $\mathbf{F}$ is formulated as

$$\mathbf{F} = \begin{bmatrix} \mathbf{I}_5 & \mathbf{I}_5 & \mathbf{0} & \mathbf{0} \\ \mathbf{0} & \mathbf{I}_5 & \mathbf{0} & \mathbf{0} \\ \mathbf{0} & \mathbf{0} & \mathbf{I}_4 & \mathbf{0} \\ \mathbf{0} & \mathbf{0} & \mathbf{0} & \mathbf{I}_4 \end{bmatrix}. \tag{7}$$

The state vector at snapshot k is

$$\boldsymbol{x}_k = [\boldsymbol{\mu}^{\mathrm{T}} \quad \Delta\overline{\boldsymbol{\mu}}^{\mathrm{T}} \quad \boldsymbol{\alpha}^{\mathrm{T}} \quad \boldsymbol{\phi}^{\mathrm{T}}], \tag{8}$$

where the vector $\Delta\overline{\boldsymbol{\mu}}$ contains the velocities of the structural parameters in $\boldsymbol{\mu}$. Here, we intentionally decouple the phase evolution from the MPC tracking to preserve the unique mapping between the phase shift and the distance d_l. The evolution of the state vector from one snapshot to the next is modelled as

$$\begin{aligned} \boldsymbol{\mu}_k &= \boldsymbol{\mu}_{k-1} + \Delta\overline{\boldsymbol{\mu}}_{k-1} + \boldsymbol{v}_{\boldsymbol{\mu}_k} \\ \Delta\boldsymbol{\mu}_k &= \Delta\overline{\boldsymbol{\mu}}_{k-1} + \boldsymbol{v}_{\Delta\overline{\boldsymbol{\mu}}_k} \\ \boldsymbol{\alpha}_{i,k} &= \boldsymbol{\alpha}_{i,k-1} + \boldsymbol{v}_{\boldsymbol{\alpha}_k} \\ \boldsymbol{\phi}_{i,k} &= \boldsymbol{\phi}_{i,k-1} + \boldsymbol{v}_{\boldsymbol{\phi}_k}, \end{aligned} \tag{9}$$

where $\boldsymbol{v}_{[\,.\,]}$ denotes the state noise vector. The selection and tuning of process noise variance are very important especially for the narrowband case, because the orthogonality is not tightly held between close-by MPCs. Small variance may lead to smooth but slow tracking, and some small movements might be missed. Large variance enables quick response to non-smooth movements like sharp turns, but with high risk of phase slip. Hence, a trade-off is needed. Here, we follow the guideline that the value of $\boldsymbol{v}_{\Delta\overline{\boldsymbol{\mu}}_k}$ should be in the same order as the maximum acceleration magnitude [6]. The complex path weight is assumed to be slowly varying and to account for larger changes in the propagation processes, e.g., reflection, scattering, etc. Reinitializations of $\boldsymbol{\gamma}_l$ are sometimes needed in the tracking process [3].

III. Propagation Path Parameters Estimation

As shown in the proposed framework (Fig. 1), the MPC parameters are estimated with an EKF. We realize that an accurate initial state estimation is a prerequisite for the fast convergence and accurate tracking in the EKF. In this work,

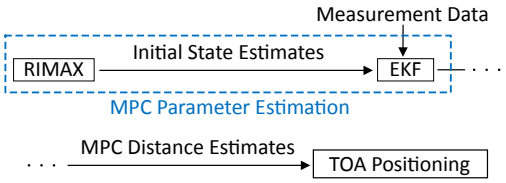

Fig. 1. Proposed positioning framework.

the RIMAX algorithm is applied to the first snapshot for the initial estimates of MPC parameters and noise covariance [4]. Besides, the state dimension adjustment is performed alongside the EKF iteration.

A. Initialization with RIMAX

Firstly, MPC detection is performed with a successive path cancellation framework, where the maximum-likelihood (ML)-based 3D-grid approach is used. Each detected path is further optimized locally. This detection framework uses oversampling to enhance delay and angle resolution, therefore closely located MPCs could be detected.

After subtracting the specular-like components, the residual is considered as the colored noise process with a covariance matrix $\mathbf{R}$, which consists of the measurement noise following a Gaussian distribution $\mathcal{N}(0,\, \sigma^2\mathbf{I})$, and the DMC. The DMC is modelled stochastically and the covariance matrix has a shifted Kronecker structure, which is computationally efficient especially when a large antenna array is used [7]. The full noise covariance matrix is given by

$$\mathbf{R} = \mathbf{R}_{\mathrm{R}} \otimes \mathbf{R}_{\mathrm{T}} \otimes \mathbf{R}_f + \sigma^2\mathbf{I}, \tag{10}$$

where $\mathbf{R}_f \in \mathbb{C}^{N_f \times N_f}$ is the covariance matrix in the frequency domain with Toeplitz structure. We observed that the power delay profile of the residual shows a spatially white characteristic at the base station (BS) side, therefore the covariance matrices $\mathbf{R}_{\mathrm{T}} \in \mathbb{C}^{N_{\mathrm{Tx}} \times N_{\mathrm{Tx}}}$ and $\mathbf{R}_{\mathrm{R}} \in \mathbb{C}^{N_{\mathrm{Rx}} \times N_{\mathrm{Rx}}}$, which describe the angular distributions at the transmit and receive sides respectively, are assumed as identity matrices in this implementation.

The structural vectors of MPCs and the parameter set of DMC are optimized alternatingly with the Levenberg-Marquardt algorithm and the ML-Gauss-Newton algorithm, respectively. The details can be found in [4].

B. Extended Kalman Filter

The path parameters are tracked with an EKF [3]. Due to the non-linear channel model used, we firstly linearize the data model $\mathbf{h}_{sp}(\mathbf{x})$ by taking the first-order partial derivatives over the state vector, which gives the Jacobian matrix as

$$\mathbf{D}(\mathbf{x}) = \frac{\partial \mathbf{h}_{sp}(\mathbf{x})}{\partial \mathbf{x}^{\mathrm{T}}}. \tag{11}$$

The first-order and the second-order partial derivative of the log-likelihood function, i.e., the score function $\mathbf{q}$ and the Fisher information matrix $\mathbf{J}$, are also needed in the iteration. These are computed as

$$\mathbf{q}(\mathbf{h}|\mathbf{x}, \mathbf{R}) = 2 \cdot \Re\left\{\mathbf{D}^{\mathrm{H}}(\mathbf{x})\mathbf{R}^{-1}(\mathbf{h} - \mathbf{h}_{sp}(\mathbf{x}))\right\}, \tag{12}$$

$$\mathbf{J}(\mathbf{x}, \mathbf{R}) = 2 \cdot \Re\left\{\mathbf{D}^{\mathrm{H}}(\mathbf{x})\mathbf{R}^{-1}\mathbf{D}(\mathbf{x})\right\}. \tag{13}$$

The procedure of the EKF is summarized as

$$\hat{\mathbf{x}}_{(k|k-1)} = \mathbf{F}\hat{\mathbf{x}}_{(k-1|k-1)}, \tag{14}$$

$$\mathbf{P}_{(k|k-1)} = \mathbf{F}\mathbf{P}_{(k-1|k-1)}\mathbf{F}^{\mathrm{T}} + \mathbf{Q}, \tag{15}$$

$$\mathbf{P}_{(k|k)} = (\mathbf{P}^{-1}_{(k|k-1)} + \mathbf{J})^{-1}, \tag{16}$$

$$\Delta\hat{\mathbf{x}}_{(k)} = \mathbf{P}_{(k|k)}\mathbf{q}, \tag{17}$$

$$\hat{\mathbf{x}}_{(k|k)} = \hat{\mathbf{x}}_{(k|k-1)} + \Delta\hat{\mathbf{x}}_{(k)}, \tag{18}$$

where $\mathbf{P}_{(k|k-1)}$ and $\mathbf{P}_{(k|k)}$ are the filter error covariances denoting the prediction and update uncertainties of the state vector, respectively.

C. State Dimension Adjustment

In channel sounding, the number of co-existing propagation paths varies over time. The detection and elimination (death-birth) of paths are assumed to be statistically independent and performed alongside the EKF iteration with two separate steps. The first step is to remove unreliable paths by evaluating the relative variance of each path [4], defined as

$$\mathrm{var}_r = \sum_{p=1}^{N_p} \frac{\mathrm{var}_{\gamma_p}}{|\,\gamma_p\,|^2} < \varepsilon_r, \tag{19}$$

where γ_p is the magnitude of the estimated path weight of polarization $p \in \{\mathrm{HH}, \mathrm{HV}, \mathrm{VH}, \mathrm{VV}\}$ and var_{γ_p} is the estimation error variance extracted from the filtering error covariance matrix. Intuitively, var_r should be smaller than 0 dB, which indicates that the certainty of the magnitude estimation should be larger than its uncertainty. A reliability check is performed every 30 snapshots and only paths with var_r smaller than the threshold ε_r are preserved in the state for further tracking. Hence, the MPC lifetime is here defined as the time duration that the relative variance of a MPC is below a given threshold, which is geometry-independent in this sense. The next step is to detect new paths. We limit the number of newly initialized MPCs in each snapshot to control the model complexity and reduce the interference between coherent paths [4].

IV. Measurement Campaign

This framework is designed for the multiple-input multiple-output (MIMO) case where angular information is available from both sides. However, UEs with single or few antennas are more common in practice and the lack of AODs makes the path estimation and tracking a harder problem. To test the performance of the proposed framework in a real but controlled environment, a measurement campaign was performed in a large sports hall with the RUSK LUND channel sounder. Fig. 2 shows an overview of the measurement area. A cylindrical antenna array with 128 ports (Fig. 3a) is used as BS at the Rx side, the center of which is 1.42 m above the ground. A conical monopole omnidirectional antenna (Fig. 3b) is used to represent a UE at the Tx side. The distance between UE and BS is around 17 m and line-of-sight (LOS) conditions apply. The transfer functions were recorded at a center frequency

Fig. 2. Overview of the measurement area in the sports hall, Medicon Village, Lund, Sweden. Room dimension is around 20 m × 36 m × 7.5 m.

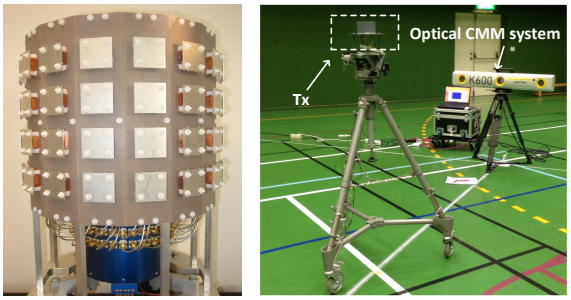

Fig. 3. (a) The cylindrical antenna array at the Rx side; (b) The conical monopole omnidirectional antenna at the Tx side and the optical CMM system.

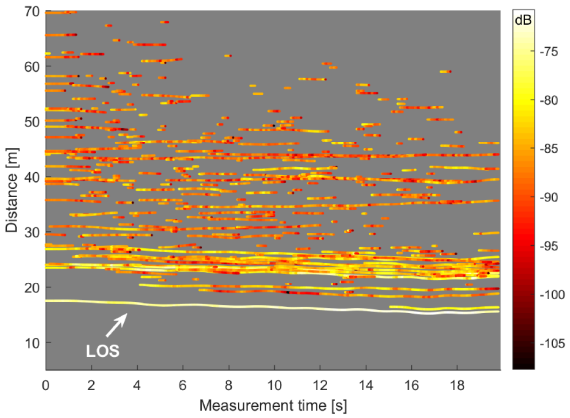

Fig. 4. The tracked absolute propagation distances of MPCs. The color indicates the power in dB scale.

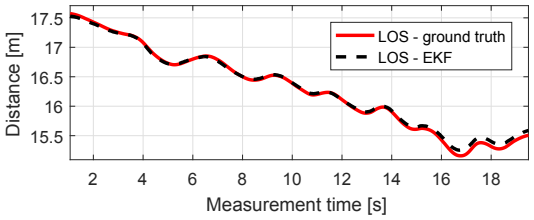

Fig. 5. Performance evaluation of the tracked LOS component.

around 2.7 GHz and with a signal bandwidth of 40 MHz. To avoid large variation of path parameters, especially the phase slip between two consecutive snapshots, the spatial sampling rate of the wireless channel was sufficiently high. In total, 6000 channel snapshots were collected in 19.7 s. The Tx was placed on a tripod and manually moved to write the "**Lund**" letters in a 2 m^3 space. Meanwhile, an optical coordinate measuring machine (CMM) system (Fig. 3b) was used to capture the UE motion with accuracy down to millimeter, which acts as the ground truth for performance analysis.

V. MPC Tracking Results and Analysis

This section focuses on the performance of MPC tracking results. Fig. 4 shows the tracked propagation distances of MPCs from the EKF implementation. It could be observed that the LOS component with the distance around 17 m is tracked steadily since the beginning. About 2 m apart from the LOS is the ground reflection path which is tracked shortly in the end. Besides, many other MPCs with long lifetimes could also be observed in the range of 20-70 m propagation distance. For better evaluation of the tracking performance, we zoom into the LOS component and compare the distance estimates with the ground truth. The black dashed line denotes the distance estimates from EKF. The red solid line in Fig. 5 is the true propagation distance of the LOS component which is calculated based on the 3D coordinates from the optical system and the coordinates of the BS. The two curves are manually time synchronized for better comparison. As shown from the comparison, the EKF could catch all the movements of the UE, even some fine ones and sharp turns. The estimates have a good match with the ground truth most of the time, besides some deviations observed after 16 s. The biggest deviation from the ground truth is about 8 cm. The MPCs located in the same delay bin as the LOS component are correlated and they show degraded quality of tracking.

We further analyzed the angular-power distribution of the tracked MPCs. The MPCs are plotted in a 3D coordinate system based on the estimates of distances and azimuth/elevation AOAs without considering the interaction order. The top view (Fig. 6a) shows that the tracked MPCs are distributed over the entire azimuth domain and paths are intensively detected in the similar direction as the LOS component. From the vertical distribution (Fig. 6b), a few paths are observed from the ground or at similar height as the BS, but most of the paths are from the complex ceiling structure of the room, e.g., the metal beams of the ceiling in Fig. 2. Those complex room structures would bring additional uncertainties to the distance estimates. Moreover, the similar behaviour of the long-tracked MPCs in the angular domain may become a challenge for 3D positioning, for which the MPCs with sparse angles are preferred. However, it is interesting to see the performance in the real but non-ideal case.

Ghost components around some high-power MPCs are observed during the tracking. They usually have similar angles and propagation distances as the dominant MPCs close by and experience very short lifetimes. These components are mainly generated due to power compensation in the estimation

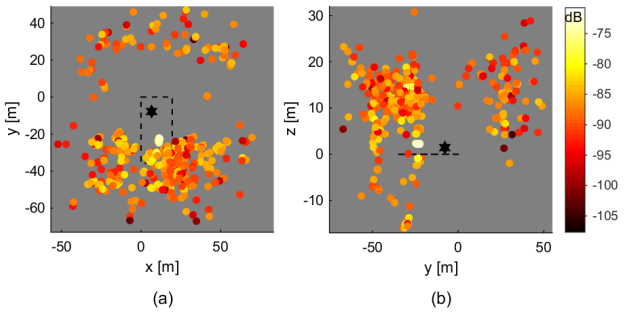

Fig. 6. 3D plot of the tracked MPCs. Black dashed line denotes the room geometry and the hexagram represents the location of BS. The top-view plot (a) shows how tracked MPCs distributed in the azimuth plane. The side-view plot (b) shows the vertical distribution.

procedure and do not have actual physical meaning, therefore they are not considered in the following positioning step.

VI. Positioning Algorithm and Results

As seen in Fig. 4 and Fig. 5, most of the MPCs can only be observed during fractions of the measurement duration and the estimation quality is not consistent during the whole tracking process for an individual MPC, i.e., there are outliers in the data for which the errors are substantial. Therefore, the question here is how to optimize the positioning performance in the presence of missing data and outliers, which is a highly non-convex problem.

A. Mathematical Formulation of Geometrical Problem

A few assumptions are firstly given for modeling the geometrical problem. The tracked MPCs from EKF are numbered with $i = 1, 2, \ldots, m$, where $i = 1$ represents the LOS component. These paths are assumed to originate from n UE positions $\mathbf{Tx}_j \in \mathbb{R}^3$, $j = 1, \ldots, n$. The BS is stationary at position $\mathbf{Rx}_1 \in \mathbb{R}^3$. To formulate the measured distances, we assume that the tracked MPCs are reflected from planar surfaces and mirror the BS, i.e., each MPC can be considered as being received at a mirrored BS position $\mathbf{Rx}_i$. The distance estimates are only given for a set I of (i, j) combinations due to missing data. As it will be shown, the errors of outliers in the distance estimates are substantial. However, for a large amount of distance estimates the errors are fairly small (in the order of a few centimeters). The measured distances are then

$$d_{ij} = \|\mathbf{Rx}_i - \mathbf{Tx}_j\|_2 + \epsilon_{ij}, \forall (i,j) \in I, \tag{20}$$

where $\epsilon_{ij} \in N(0, \sigma^2_{inl})$ for $(i, j) \in I_{inl}$ and ϵ_{ij} are drawn from an unknown distribution for $(i, j) \in I_{outl}$. This distribution has a significantly larger variance. One useful approach is to minimize the negative log likelihood. To simplify the problem, we assume that the negative log likelihood for the outliers is a constant, i.e., each outlier gives the same penalty. In this way the problem becomes an optimization problem.

***Problem** 1:* (Time-of-Arrival Self-Calibration) Given absolute distance estimates $d_{ij} \forall (i, j) \in I$, find the inlier set $I_{inl} \subset I$, the UE positions $\mathbf{Tx}_j \in \mathbb{R}^3$ and the mirrored BS positions $\mathbf{Rx}_i \in \mathbb{R}^3$ that solves the following optimization problem

$$\min_{I_{inl}, \mathbf{Rx}_i, \mathbf{Tx}_j} \sum_{(i,j) \in I_{inl}} (d_{ij} - \|\mathbf{Rx}_i - \mathbf{Tx}_j\|_2)^2 + \sum_{(i,j) \in I_{outl}} C, \tag{21}$$

where $I_{outl} = I \setminus I_{inl}$. This is a highly non-linear, non-convex optimization problem. The problem changes character if both $\mathbf{Tx}_j$ and $\mathbf{Rx}_j$ span 3D, or either one of them or both are restricted to a plane or a line as shown in [8]. The problem is ill-defined if there is too little data. For planar problems we require $m \geq 3, n \geq 3$, [9]. For 3D problems more data is needed, typically $m \geq 4, n \geq 6$, [10]. Algorithms for solving Problem 1 using hypothesize and test paradigm are presented in [11].

B. Estimation of the Distance Estimates Error Distribution and Mirrored BS Positions

The modified version of Problem 1 where say the transmitter positions $\mathbf{Tx}_j$ are known, is a substantially better conditioned problem. In this case, we can solve for

$$\min_{I_{inl}, \mathbf{Rx}_i} \sum_{i|(i,j) \in I_{inl}} (d_{ij} - \|\mathbf{Rx}_i - \mathbf{Tx}_j\|_2)^2 + \sum_{i|(i,j) \in I_{outl}} C \tag{22}$$

independently for each mirrored BS position $\mathbf{Rx}_i$. This can be done by using Random Sample Consensus (RANSAC) [12].

The resulting residuals $d_{ij} - \|\mathbf{Rx}_i - \mathbf{Tx}_j\|_2$ can be used to empirically assess properties of the error distribution. We selected those paths that were longer than 500 snapshots from the tracked $m = 282$ MPCs, which gave a set of 50 MPCs. For each of them, we estimated the mirrored BS position using RANSAC (to obtain I_{inl}) followed by the non-linear optimization of (22) (to obtain $\mathbf{Rx}_i$). In total these 50 tracked MPCs gave us 103 480 distance samples, i.e., approximately 2000 each. Of these 77 490 were considered to be inliers. This gives us an estimated inlier ratio of 75%. The standard deviation of the inlier residuals is 4.6 cm.

Using the ground truth UE positions $\mathbf{Tx}_j$, we robustly initialized the LOS component receiver position, i.e., $\mathbf{Rx}_1$ as well as all the mirrored BS positions of MPCs. This was followed by non-linear refinement. The reconstructed BS position $\mathbf{Rx}_1$ along with some examples of the mirrored BS positions are shown in Fig. 7. It could be observed that the estimated BS position is located close to the true position, and the mirrored BS positions look plausible.

C. Estimation of UE Positions

We now target the full version of Problem 1, where the UE positions, the BS position and all the mirrored BS positions are unknown. To make this highly complex estimation problem tractable, two assumptions are made here. Firstly, $\mathbf{Tx}_j$ are assumed to be constrained in a plane, because the UE was moved approximately in a plane in the measurement. Secondly, we assume that we know which distance estimates are inliers. This problem is then proceeded by splitting the whole dataset in a number of smaller segments in time, which results in

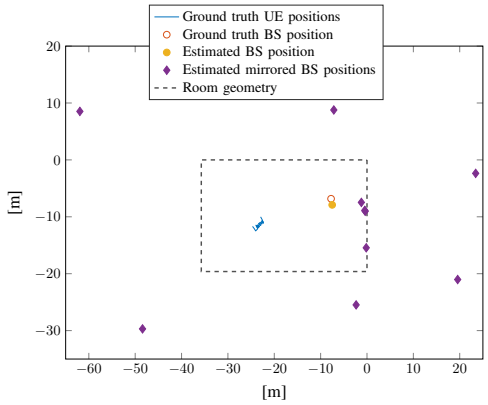

Fig. 7. Robust estimation of BS position and mirrored BS positions using the ground truth UE positions.

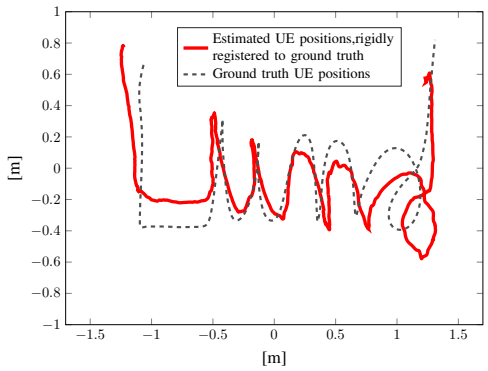

Fig. 8. The ground truth (dashed-grey) and the estimated UE positions (red). Note that this estimation is only based on the distance estimates and no ground truth UE positions are used.

117 segments of length 100 snapshots with 50 snapshots overlap between adjacent segments. For each segment, we robustly initialized both $\mathbf{Rx}_j$ and $\mathbf{Tx}_j$ using minimal solvers and RANSAC [8] based only on the distance estimates from the EKF. This is followed by non-linear optimization. The different solutions from the 117 segments were then registered into a common coordinate system using the overlap between segments. The estimated UE positions (in red) is shown in Fig. 8. Also shown (in dashed grey) is the ground truth. The two trajectories have been rigidly registered to each other. It could be observed that the estimated trajectory shows a clear "**Lund**"-word pattern, with all the fine movements details caught. However, the overall shape is stretched along the diagonal direction, which results in a larger deviation from the ground truth especially in the beginning and the end. The largest deviation of the estimated UE position from the ground truth happens at the sharp turn of "**L**", which is 26 cm, and the overall mean deviation is 13 cm. The main reason of the stretch problem is that many MPCs are tracked in a similar direction as the LOS component, as shown in Fig. 6. The similar behaviour of MPCs in the angular domain will cause the estimated UE positions to be scaled or projected.

VII. Summary and Conclusion

In this paper, we introduced and showed a proof-of-concept for a robust phase-based positioning framework using massive MIMO. MPC parameters, e.g., phase-based distance and angle, are estimated and tracked with an EKF. A TOA self-calibration positioning algorithm is then used for trajectory estimation. The positioning results of a 2D complex movement measurement show that the proposed positioning framework could achieve outstanding positioning performance even with standard cellular bandwidths. Besides, no prior knowledge of the surroundings is needed, so the framework could be easily applied in different environments given that there are enough many scatterers present. To sum up, phase-based positioning using massive MIMO is a promising high-resolution positioning solution for current and next generation cellular systems.

VIII. Acknowledgements

The authors would like to thank Erik Leitinger, Jose Flordelis, Joao Vieira and Christian Nelson for helping with the measurements. We would also like to acknowledge the support from Björn Olofsson with the motion capture system. This work was supported by the Swedish Research Council VR and the strategic research area ELLIIT.

References

[1] E. Leitinger, P. Meissner, M. Lafer, and K. Witrisal, "Simultaneous localization and mapping using multipath channel information," in *2015 IEEE International Conference on Communication Workshop (ICCW)*, June 2015, pp. 754–760.

[2] M. Zhu, J. Vieira, Y. Kuang, K. Åström, A. F. Molisch, and F. Tufvesson, "Tracking and positioning using phase information from estimated multi-path components," in *2015 IEEE International Conference on Communication Workshop (ICCW)*, June 2015, pp. 712–717.

[3] J. Salmi, A. Richter, and V. Koivunen, "Detection and tracking of mimo propagation path parameters using state-space approach," *IEEE Transactions on Signal Processing*, vol. 57, no. 4, pp. 1538–1550, 2009.

[4] A. Richter, "Estimation of radio channel parameters: Models and algorithms," Ph.D. dissertation, Technischen Universität Ilmenau, Fakultät für Elektrotechnik und Informationstechnik, 2005.

[5] A. F. Molisch, *Wireless Communications*, 2nd ed. New York, USA: Wiley Publishing, 2011.

[6] Y. Bar-Shalom and X.-R. Li, *Estimation with Applications to Tracking and Navigation*. New York, NY, USA: John Wiley & Sons, Inc., 2001.

[7] J. Salmi, "Contributions to measurement-based dynamic MIMO channel modeling and propagation parameter estimation," Ph.D. dissertation, Helsinki University of Technology, Finland, 2009. [Online]. Available: https://aaltodoc.aalto.fi/handle/123456789/4638

[8] S. Burgess, Y. Kuang, and K. Åström, "TOA sensor network self-calibration for receiver and transmitter spaces with difference in dimension," *Signal Processing*, vol. 107, pp. 33–42, 2015.

[9] H. Stewénius, "Gröbner basis methods for minimal problems in computer vision," Ph.D. dissertation, Lund University, Apr. 2005.

[10] Y. Kuang, S. Burgess, A. Torstensson, and K. Åström, "A complete characterization and solution to the microphone position self-calibration problem," in *The 38th International Conference on Acoustics, Speech, and Signal Processing*, 2013.

[11] K. Batstone, M. Oskarsson, and K. Åström, "Robust time-of-arrival self calibration with missing data and outliers," in *2016 24th European Signal Processing Conference (EUSIPCO)*, Aug 2016, pp. 2370–2374.

[12] M. A. Fischler and R. C. Bolles, "Random sample consensus: A paradigm for model fitting with applications to image analysis and automated cartography," *Commun. ACM*, vol. 24, no. 6, pp. 381–395, Jun. 1981. [Online]. Available: http://doi.acm.org/10.1145/358669.358692